Letter

Pole determination of $P^{\Lambda}_{\psi s}(4338)$ and possible $P^{\Lambda}_{\psi s}(4255)$ in $B^- \to J/\psi\Lambda\bar{p}$

S. X. Nakamura[1,2,*] and J.-J. Wu[3,†]

[1]*University of Science and Technology of China, Hefei 230026, People's Republic of China*
[2]*State Key Laboratory of Particle Detection and Electronics (IHEP-USTC), Hefei 230036, People's Republic of China*
[3]*School of Physical Sciences, University of Chinese Academy of Sciences (UCAS), Beijing 100049, China*

(Received 30 August 2022; revised 28 February 2023; accepted 21 June 2023; published 14 July 2023)

The first hidden-charm pentaquark candidate with strangeness, $P^{\Lambda}_{\psi s}(4338)$, was recently discovered in $B^- \to J/\psi\Lambda\bar{p}$ by the LHCb Collaboration. $P^{\Lambda}_{\psi s}(4338)$ shows up as a bump at the $\Xi_c\bar{D}$ threshold in the $J/\psi\Lambda$ invariant mass ($M_{J/\psi\Lambda}$) distribution. The $M_{J/\psi\Lambda}$ distribution also shows a large fluctuation at the $\Lambda_c\bar{D}_s$ threshold, hinting the existence of a possible $P^{\Lambda}_{\psi s}(4255)$. In this work, we determine the $P^{\Lambda}_{\psi s}(4338)$ and $P^{\Lambda}_{\psi s}(4255)$ pole positions for the first time. For this purpose, we fit a $B^- \to J/\psi\Lambda\bar{p}$ model to the $M_{J/\psi\Lambda}$, $M_{J/\psi\bar{p}}$, $M_{\Lambda\bar{p}}$, and $\cos\theta_{K^*}$ distributions from the LHCb simultaneously; $\chi^2/\mathrm{ndf} \sim 1.21$. Then we extract $P^{\Lambda}_{\psi s}$ poles from a unitary $\Xi_c\bar{D}$-$\Lambda_c\bar{D}_s$ coupled-channel scattering amplitude built in the model. In our default fit, the $P^{\Lambda}_{\psi s}(4338)$ pole is found at (4338.2 ± 1.4)–$(1.9 \pm 0.5)i$ MeV while the $P^{\Lambda}_{\psi s}(4255)$ pole at 4254.7 ± 0.4 MeV. The $P^{\Lambda}_{\psi s}(4338)$ and $P^{\Lambda}_{\psi s}(4255)$ are mostly $\Xi_c\bar{D}$ bound and $\Lambda_c\bar{D}_s$ virtual states, respectively. Through our analysis, the data disfavors a hypothesis of $P^{\Lambda}_{\psi s}(4338)$ as merely a kinematical effect. This pole determination, which is important in its own right, sets a primary basis to study the nature of the $P^{\Lambda}_{\psi s}$ states.

DOI: 10.1103/PhysRevD.108.L011501

I. INTRODUCTION

Since the foundation of the quark model, we have been addressing the fundamental question; "What form of the matter can be built from quarks?" Recent experimental discoveries of pentaquark and tetraquark candidates have decisively widened our territory of the conventional qqq and $q\bar{q}$ hadrons to include qualitatively different $qqqq\bar{q}$, $qq\bar{q}\,\bar{q}$, and even more exotic structures; see reviews [1–8]. Establishing the (non)existence of pentaquark and tetraquark states is now essential to answer the above fundamental question.

The existence of hidden-charm pentaquarks with strangeness ($P^{\Lambda}_{\psi s}$, $udsc\bar{c}$) has been expected theoretically [9–11], and the discovery of hidden-charm pentaquark candidates ($uudc\bar{c}$) [12,13] further strengthened the expectation [14–19]. The first evidence (3.1σ) of $P^{\Lambda}_{\psi s}$ was found, by the LHCb Collaboration, in $\Xi_b^- \to J/\psi\Lambda K^-$ as a bump at $\sim$4459 MeV in the $J/\psi\Lambda$ invariant mass ($M_{J/\psi\Lambda}$) distribution [20]. This result invited lots of theoretical studies on $P^{\Lambda}_{\psi s}(4459)$ [21–35]. Then, very recently, the LHCb announced the first discovery ($> 10\sigma$) of $P^{\Lambda}_{\psi s}$ in $B^- \to J/\psi\Lambda\bar{p}$ [36]. Their amplitude analysis determined the $P^{\Lambda}_{\psi s}$ mass, width, and spin-parity as 4338.2 ± 0.7 MeV, 7.0 ± 1.2 MeV, and $J^P = 1/2^-$, respectively. In response to the discovery, proposals have been made to interpret $P^{\Lambda}_{\psi s}(4338)$ as a $\Xi_c\bar{D}$ molecule [37–39] and as a triangle singularity [40].

To understand the nature of $P^{\Lambda}_{\psi s}(4338)$, its properties such as the mass, width, and J^P are the crucial information. The LHCb amplitude analysis obtained them under an assumption that the $P^{\Lambda}_{\psi s}(4338)$ peak is due to a resonance that can be well-simulated by a Breit-Wigner (BW) amplitude. However, the $P^{\Lambda}_{\psi s}(4338)$ peak is located right on the $\Xi_c\bar{D}$ threshold [see Fig. 3(a)], which would invalidate this assumption. First of all, the resonancelike structure might be caused by a kinematical effect (threshold cusp) and not by a resonance pole [41]. If a $P^{\Lambda}_{\psi s}(4338)$ pole exists and it couples with $\Xi_c\bar{D}$, the BW amplitude is still not suitable since it does not account for: (i) the width starts to increase rapidly as the $\Xi_c\bar{D}$ channel opens; (ii) the line shape due to the pole can be distorted by the branch point (threshold) of the complex energy plane where the pole is located. The relevance of the items (i) and (ii) was demonstrated in Ref. [42].

*satoshi@ustc.edu.cn
†wujiajun@ucas.ac.cn

What needs to be done is to replace the BW approximation with the proper pole-extraction method where a unitary coupled-channel amplitude is fitted to the data, and poles on relevant Riemann sheets are searched by analytically continuing the amplitude. This is the main task in this paper. The pole value not only provides important knowledge reflecting the QCD dynamics but also serves as a basis for studying the nature of $P^{\Lambda}_{\psi s}(4338)$.

Meanwhile, the $M_{J/\psi\Lambda}$ distribution data shows a large fluctuation at $M_{J/\psi\Lambda} \sim 4255$ MeV. The LHCb examined this fluctuation as a possible $P^{\Lambda}_{\psi s}(4255)$ contribution, and found it statistically insignificant. However, the fluctuation occurs at the $\Lambda_c\bar{D}_s$ threshold where a visible threshold cusp would be expected from a color-favored $B^- \to \Lambda_c\bar{D}_s\bar{p}$ followed by $\Lambda_c\bar{D}_s \to J/\psi\Lambda$. A $\Lambda_c\bar{D}_s$ rescattering might cause a pole to enhance the cusp.

In this work, we analyze the LHCb data on $B^- \to J/\psi\Lambda\bar{p}$ in detail. The $M_{J/\psi\Lambda}$, $M_{J/\psi\bar{p}}$, $M_{\Lambda\bar{p}}$, and $\cos\theta_{K^*}$ distribution data are simultaneously fitted with a model in which a unitary $\Xi_c\bar{D}$-$\Lambda_c\bar{D}_s$ coupled-channel amplitude is implemented. Based on the coupled-channel amplitude, we address the following issues: (i) the $P^{\Lambda}_{\psi s}(4338)$ pole position; (ii) a possibility that the $P^{\Lambda}_{\psi s}(4338)$ peak is merely a $\Xi_c\bar{D}$ threshold cusp; (iii) implications of the large fluctuation at the $\Lambda_c\bar{D}_s$ threshold.

II. MODEL

The LHCb data shows visible structures only around the $\Xi_c\bar{D}$, $\Lambda_c\bar{D}_s$, and $\bar{\Lambda}_cD$ thresholds. Thus it is reasonable to assume that the structures are caused by the threshold cusps that are further enhanced or suppressed by hadronic rescatterings and the associated poles [43]; see Figs. 1(a)–1(c). Other possible mechanisms are assumed to be absorbed by a direct-decay mechanism of Fig. 1(d). For the small Q-value ($\sim$130 MeV) in $B^- \to J/\psi\Lambda\bar{p}$, we consider only s-wave interactions that are expected to dominate. We confirmed that p-wave spectators in Fig. 1 hardly improve fitting the data.

We present amplitude formulas for Figs. 1(a)–1(c). The energy, momentum, and polarization vector of a particle x are denoted by E_x, $\boldsymbol{p}_x$, and $\boldsymbol{\epsilon}_x$, respectively, and particle masses are from Ref. [44]. We also denote a baryon-meson (BM) pair with J^P by $BM(J^P)$. The initial weak $B^- \to \Xi_c\bar{D}(1/2^-)\bar{p}$ vertex [Fig. 1(a)] is

$$v_1 = c^{1/2^-}_{\Xi_c\bar{D}\,\bar{p},B^-}\langle t_{\bar{D}}t^z_{\bar{D}}t_{\Xi_c}t^z_{\Xi_c}|00\rangle f^0_{\Xi_c\bar{D}}F^0_{\bar{p}B^-}, \tag{1}$$

with a complex coupling constant $c^{1/2^-}_{\Xi_c\bar{D}\,\bar{p},B^-}$. An isospin Clebsch-Gordan coefficient is given by the bracket where $t^{(z)}_x$ is the isospin (z-component) of a particle x. The $B^- \to \Lambda_c\bar{D}_s(1/2^-)\bar{p}$ [Fig. 1(b)] and $\bar{\Lambda}_cD^0(1/2^+)\Lambda$ [Fig. 1(c)] vertices are the same form with couplings $c^{1/2^-}_{\Lambda_c\bar{D}_s\bar{p},B^-}$ and $c^{1/2^+}_{\bar{\Lambda}_cD\Lambda,B^-}$. We introduced dipole form factors f^L_{ij} and F^L_{kl} defined by

$$f^L_{ij} = \frac{(1+q^2_{ij}/\Lambda^2)^{-2-\frac{L}{2}}}{\sqrt{E_iE_j}}, \quad F^L_{kl} = \frac{(1+\tilde{p}^2_k/\Lambda^2)^{-2-\frac{L}{2}}}{\sqrt{E_kE_l}}, \tag{2}$$

where q_{ij} ($\tilde{p}_k$) is the momentum of i (k) in the ij (total) center-of-mass frame. We use a common cutoff value $\Lambda = 1$ GeV in Eq. (2) for all the interaction vertices. The $B^- \to \bar{\Lambda}_cD^0\Lambda, \Lambda_c\bar{D}_s\bar{p}$ decays are color-favored processes, while $B^- \to \Xi_c\bar{D}\,\bar{p}$ is color suppressed.

The above weak decays are followed by hadronic scatterings. We take a data-driven approach to the hadron interactions while respecting the relevant coupled-channel unitarity; the idea on which the K-matrix approach is also based. We use hadron interactions in a form not biased by any particular models, and all coupling strengths are determined by the data.

We consider the most important coupled-channels: a $\Xi_c\bar{D} - \Lambda_c\bar{D}_s(1/2^-)$ coupled-channel scattering in Figs. 1(a) and 1(b), and a $\bar{\Lambda}_cD(1/2^+)$ single-channel scattering in Fig. 1(c). We assume that transitions to the $J/\psi\Lambda$ and $J/\psi\bar{p}$ channels can be treated perturbatively.

We use an s-wave meson-baryon interaction potential,

$$v_{\beta,\alpha} = h_{\beta,\alpha}\langle t_{\beta1}t^z_{\beta1}t_{\beta2}t^z_{\beta2}|TT^z\rangle\langle t_{\alpha1}t^z_{\alpha1}t_{\alpha2}t^z_{\alpha2}|TT^z\rangle \times f^0_\beta Y_{00}f^0_\alpha Y_{00}, \tag{3}$$

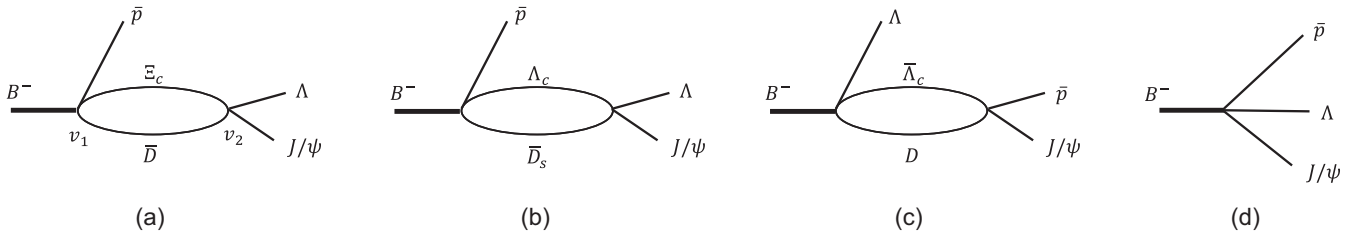

FIG. 1. $B^- \to J/\psi\Lambda\bar{p}$ mechanisms initiated by weak vertex v_1 of (a) $B^- \to \Xi_c\bar{D}\,\bar{p}$, (b) $B^- \to \Lambda_c\bar{D}_s\bar{p}$, (c) $B^- \to \bar{\Lambda}_cD\Lambda$, and (d) $B^- \to J/\psi\Lambda\bar{p}$. The second vertex v_2 in (a,b) [(c)] includes a $\Xi_c\bar{D} - \Lambda_c\bar{D}_s$ coupled-channel [$\bar{\Lambda}_cD$ single-channel] scattering, followed by a perturbative transition to $J/\psi\Lambda$ [$J/\psi\bar{p}$].

where α and β label coupled-channels such as $\Xi_c\bar{D}(1/2^-)$, and $\alpha 1$ and $\alpha 2$ are the meson and baryon in a channel α, respectively; $h_{\beta,\alpha}$ is a coupling constant; Y_{lm} denotes a spherical harmonics. We introduce $[G^{-1}(E)]_{\beta\alpha} = \delta_{\beta\alpha} - h_{\beta,\alpha}\sigma_\alpha(E)$ with

$$\sigma_\alpha(E) = \sum_{t^z} \int dq q^2 \frac{\langle t_{\alpha 1} t^z_{\alpha 1} t_{\alpha 2} t^z_{\alpha 2} | TT^z\rangle^2 [f^0_\alpha(q)]^2}{E - E_{\alpha 1}(q) - E_{\alpha 2}(q) + i\varepsilon}, \quad (4)$$

where $\sum_{t^z}$ is needed for $\alpha = \Xi_c\bar{D}$; $\Xi_c^+ D^-$ and $\Xi_c^0\bar{D}^0$ intermediate states with the charge-dependent masses are included. The perturbative interactions for $\Xi_c\bar{D}(1/2^-)$, $\Lambda_c\bar{D}_s(1/2^-) \to J/\psi\Lambda$ and $\bar{\Lambda}_c D^0(1/2^+) \to J/\psi\bar{p}$ are given by s-wave separable interactions,

$$v_{\gamma,\alpha} = h_{\gamma,\alpha}\langle t_{\alpha 1} t^z_{\alpha 1} t_{\alpha 2} t^z_{\alpha 2} | TT^z\rangle \boldsymbol{\sigma}\cdot\boldsymbol{\epsilon}_\psi f^0_\gamma Y_{00} f^0_\alpha Y_{00}, \quad (5)$$

where $\gamma = J/\psi\Lambda$ or $J/\psi\bar{p}$, and $\boldsymbol{\sigma}$ is the Pauli matrix.

With the above ingredients, following the time-ordered perturbation theory, the amplitudes are given as

$$A^{\rm loop}_{\psi\Lambda(1/2^-)} = \sum_{\alpha,\beta}^{\Xi_c\bar{D},\Lambda_c\bar{D}_s} h_{\psi\Lambda,\beta} c^{1/2^-}_{\alpha\bar{p},B^-} \boldsymbol{\sigma}\cdot\boldsymbol{\epsilon}_\psi f^0_{\psi\Lambda}(p_\psi)\sigma_\beta(M_{\psi\Lambda}) \times G_{\beta\alpha}(M_{\psi\Lambda}) F^0_{\bar{p}B^-}, \quad (6)$$

for Figs. 1(a) and 1(b), and

$$A^{\rm loop}_{\psi\bar{p}(1/2^+)} = h_{\psi\bar{p},\bar{\Lambda}_c D} c^{1/2^+}_{\bar{\Lambda}_c D\Lambda,B^-} \boldsymbol{\sigma}\cdot\boldsymbol{\epsilon}_\psi f^0_{\psi\bar{p}}(p_\psi)\sigma_{\bar{\Lambda}_c D}(M_{\psi\bar{p}}) \times G_{\bar{\Lambda}_c D,\bar{\Lambda}_c D}(M_{\psi\bar{p}}) F^0_{\Lambda B^-}, \quad (7)$$

for Fig. 1(c). The spinors of the final Λ and $\bar{p}$ implicitly sandwich the above expressions.

Regarding the color-suppressed direct decay mechanism of Fig. 1(d), we find the following $J/\psi\bar{p}(1/2^+)$ partial wave amplitude gives a reasonable fit,

$$A^{\rm dir}_{\psi\bar{p}(1/2^+)} = c^{1/2^+}_{\psi\bar{p}\Lambda,B^-} \boldsymbol{\sigma}\cdot\boldsymbol{\epsilon}_\psi f^0_{\psi\bar{p}} F^0_{\Lambda B^-}, \quad (8)$$

with a coupling constant $c^{1/2^+}_{\psi\bar{p}\Lambda,B^-}$.

III. RESULTS

We use the amplitudes of Eqs. (6)–(8) to simultaneously fit the $M_{J/\psi\Lambda}$, $M_{J/\psi\bar{p}}$, $M_{\Lambda\bar{p}}$, and $\cos\theta_{K^*}$ distributions[1] from the LHCb; see Appendix B of Ref. [45] for the procedure of calculating the invariant mass distributions. Theoretical invariant mass ($\cos\theta_{K^*}$) distributions are smeared with experimental resolutions of 1 MeV (bin width of 0.05), and are further averaged over the bin width in each bin. The obtained binned theoretical distributions are used to calculate χ^2. The amplitudes include adjustable coupling constants from the weak vertices of Eqs. (1) and (8) and from hadronic interactions of Eqs. (3) and (5). We reduce the fitting parameters by setting $h_{\psi\Lambda,\Xi_c\bar{D}} = h_{\psi\Lambda,\Lambda_c\bar{D}_s}$ since the fit quality does not significantly change by allowing $h_{\psi\Lambda,\Xi_c\bar{D}} \neq h_{\psi\Lambda,\Lambda_c\bar{D}_s}$. Then we adjust the products such as $h_{\psi\Lambda,\alpha} c^{1/2^-}_{\Xi_c\bar{D}\,\bar{p},B^-}$ in Eqs. (6) and (7). Numerical values for the coupling constants determined by the fit are given in the Supplemental Material [46]. Our default model has nine fitting parameters in total, considering that the magnitude and phase of the full amplitude are arbitrary.

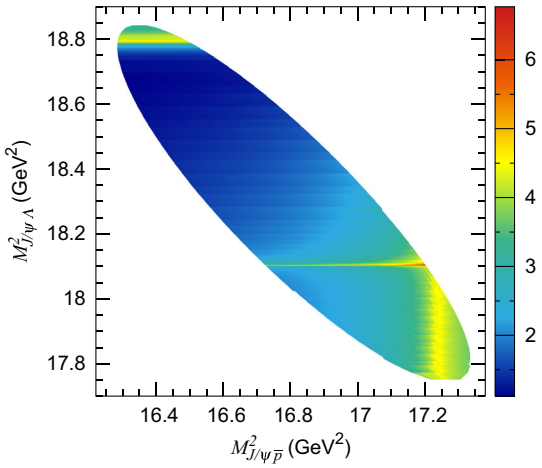

FIG. 2. $B^- \to J/\psi\Lambda\bar{p}$ Dalitz plot distribution from the default model. No smearing is applied.

We first present a Dalitz plot distribution from the default model in Fig. 2. Comparing the plot with the LHCb's (Fig. 2 in Ref. [36]), the overall pattern is quite similar, except that the peak structures in our plot are sharper since no smearing with the experimental resolution is considered.

Now, we compare the default model (red histogram) with the LHCb data in Fig. 3, showing a good agreement. In particular, the $P^{\Lambda}_{\psi s}(4338)$ and possible $P^{\Lambda}_{\psi s}(4255)$ peaks in the $M_{J/\psi\Lambda}$ distribution are well-fitted. The fit quality is $\chi^2/{\rm ndf} = (50+81+112+29)/(235-9) \simeq 1.21$ where four χ^2s are from comparing with the $M_{J/\psi\Lambda}$, $M_{J/\psi\bar{p}}$, $M_{\Lambda\bar{p}}$, and $\cos\theta_{K^*}$ distributions, respectively; "ndf" is the number of bins (40 for $\cos\theta_{K^*}$ and 3×65 for the others) subtracted by the number of the fitting parameters.

We also show contributions from the diagrams of Fig. 1 each of which has a different initial weak vertex. Overall, the diagrams of Figs. 1(c) [blue] and 1(d) [brown] dominate the process. The increasing $M_{J/\psi\bar{p}}$ distribution in Fig. 3(b) is understood as the $\bar{\Lambda}_c D$ threshold cusp from Fig. 1(c).[2] Although the diagrams

[1] $\cos\theta_{K^*} \equiv \frac{\boldsymbol{p}_\Lambda\cdot\boldsymbol{p}_\psi}{|\boldsymbol{p}_\Lambda||\boldsymbol{p}_\psi|}$ in the $\Lambda\bar{p}$ center-of-mass frame.

[2] The fit favors a repulsive $\bar{\Lambda}_c D$ interaction, consistent with our previous finding from analyzing $B^0_s \to J/\psi p\bar{p}$ [48].

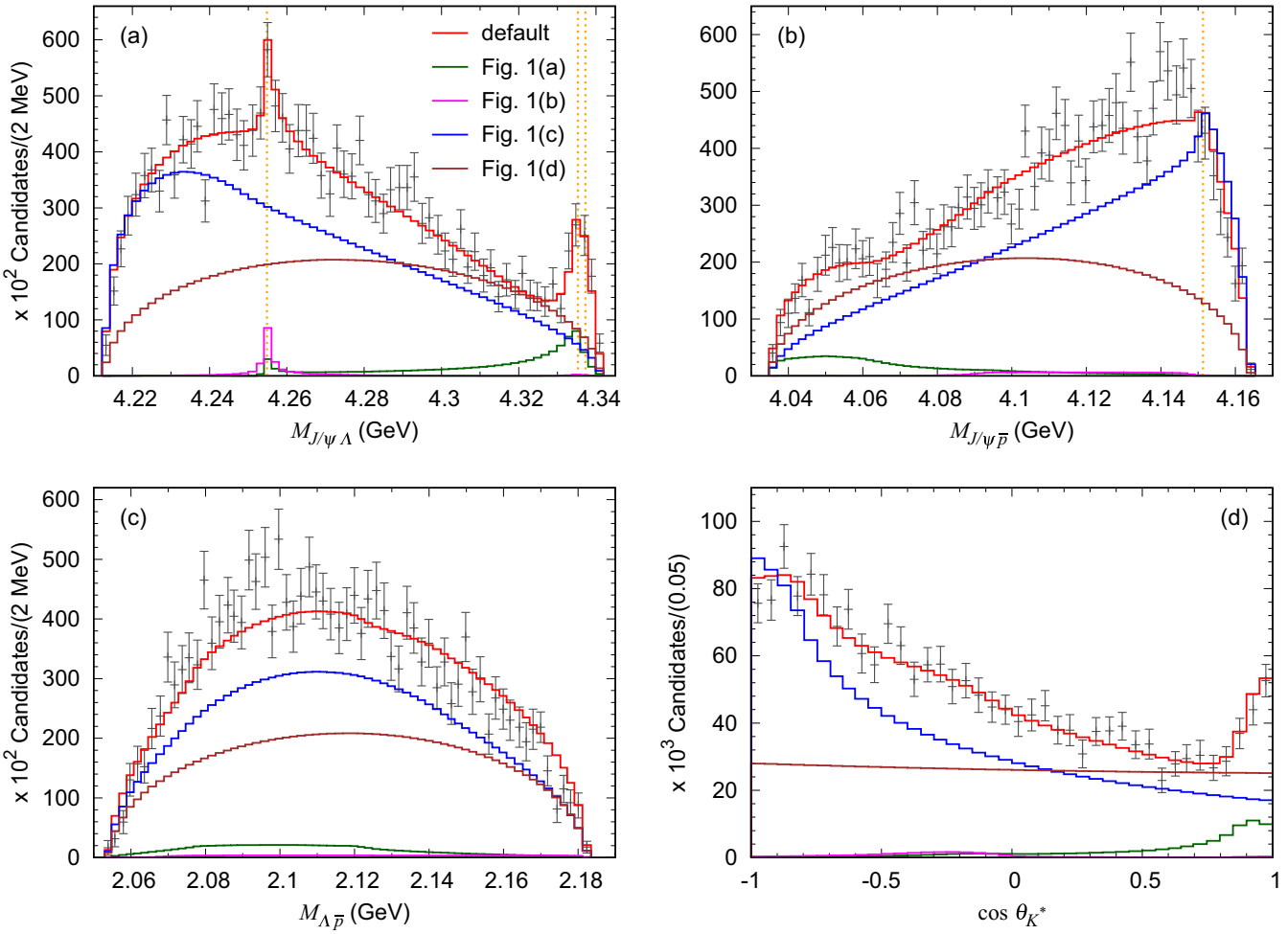

FIG. 3. (a) $J/\psi\Lambda$, (b) $J/\psi\bar{p}$, (c) $\Lambda\bar{p}$ invariant mass, and (d) $\cos\theta_{K^*}$ distributions for $B^- \to J/\psi\Lambda\bar{p}$. The default fit and contributions from different diagrams in Fig. 1 are shown. The dotted vertical lines indicate thresholds for, from left to right, $\Lambda_c^+ D_s^-$, $\Xi_c^0 \bar{D}^0$, and $\Xi_c^+ D^-$ [$\bar{\Lambda}_c^- D^0$] in the panel (a) [(b)]. Data [36] are efficiency corrected and background subtracted.

of Figs. 1(a) [green] and 1(b) [magenta] are relatively small in the magnitude, they have significantly enhanced $\Xi_c\bar{D}$ and $\Lambda_c\bar{D}_s$ threshold cusps, respectively, and develop the $P_{\psi s}^{\Lambda}$ peaks through the interference.

The large contribution from Fig. 1(c) is understandable since it is color favored. The color-suppressed Fig. 1(d) is comparable, possibly because it is not suppressed by a loop. However, the color-favored Fig. 1(b) contributes rather small. This might be because $\Lambda_c\bar{D}_s \to \Lambda J/\psi$ is suppressed compared with $\bar{\Lambda}_c D \to \bar{p}J/\psi$. The suppression would be expected since, in a meson-exchange picture, $\Lambda_c\bar{D}_s \to \Lambda J/\psi$ caused by a $D_s^{(*)}$-exchange involves $s\bar{s}$ creation and annihilation while $\bar{\Lambda}_c D \to \bar{p}J/\psi$ with a $D^{(*)}$-exchange needs light quark pair (de)excitations. Yet, a solid understanding awaits more theoretical analyses and higher statistics data.

Our default and LHCb's models describe the data rather differently. The LHCb fitted the $M_{J/\psi\bar{p}}$ distribution with a nonresonant $J/\psi\bar{p}$ [NR($J/\psi\bar{p}$)] amplitude in a polynomial form without identifying the physical origin of the increasing behavior. The NR($J/\psi\bar{p}$) includes only a $S = 3/2$ and p-wave $J/\psi\bar{p}$ to occupy ~84% fit fraction; S denotes the total spin of $J/\psi\bar{p}$. This p-wave dominance is counterintuitive since the small Q-value implies a s-wave dominance. Indeed, Figs. 1(c) and 1(d), which are dominant in our model, are s-wave $J/\psi\bar{p}$ amplitudes.

We modified our default model by replacing Figs. 1(c) and 1(d) with diagrammatically similar ones that have the same $J/\psi\bar{p}$ partial wave as the LHCb's NR($J/\psi\bar{p}$). By fitting this modified model to the LHCb data, we obtained χ^2 similar to that of the default model. However, the modified and LHCb models have line shapes qualitatively different from the default model such as (i) At the $\bar{\Lambda}_c D$ threshold in the $M_{J/\psi\bar{p}}$ distribution, our default fit has a cusp structure but our modified and the LHCb fits have a smooth line shape; (ii) Our default model (and also the LHCb data tend to) shows a plateau at $\cos\theta_{K^*} \sim -1$, but our modified and the LHCb models show a monotonically

TABLE I. $P^{\Lambda}_{\psi s}$ poles. (I) default model; (II) [(III)] alternative model with $v_{\Lambda_c\bar{D}_s,\Lambda_c\bar{D}_s}=0$ [energy dependence of Eq. (9) and $v_{\Lambda_c\bar{D}_s,\Lambda_c\bar{D}_s}=0$]. Pole positions (in MeV) and their Riemann sheets (see the text for notation) are given in the third and fourth columns, respectively.

(I)	$P^{\Lambda}_{\psi s}(4338)$	$(4338.2\pm1.4)-(1.9\pm0.5)i$	(upp)
	$P^{\Lambda}_{\psi s}(4255)$	4254.7 ± 0.4	(upp)
(II)	$P^{\Lambda}_{\psi s}(4338)$	$(4331.9\pm4.2)+(5.6\pm6.4)i$	(ppu)
		$(4328.6\pm4.2)+(4.6\pm5.9)i$	(pup)
		$(4336.1\pm1.3)+(0.3\pm1.3)i$	(puu)
(III)	$P^{\Lambda}_{\psi s}(4338)$	$(4340.0\pm8.5)-(2.2\pm8.8)i$	(upp)
		$(4340.1\pm13.3)-(5.1\pm3.5)i$	(uup)
		$(4338.0\pm4.1)-(6.2\pm7.3)i$	(uuu)

decreasing behavior. The future higher statistic data might distinguish these differences.

Also, the LHCb's model has 16 fitting parameters, in contrast to 9(8) parameters in our default model (alternative model below). Although the LHCb's model fits richer six-dimensional data, ∼2 times more parameters sound too many. The p-wave dominance and excessive parameters in the LHCb's model are possibly from missing relevant mechanisms such as Figs. 1(a)–1(c); many other mechanisms mimic the relevant ones through complicated interferences.

We searched for poles in our default $\Xi_c\bar{D}-\Lambda_c\bar{D}_s(1/2^-)$ coupled-channel scattering amplitude by the analytic continuation. We found $P^{\Lambda}_{\psi s}(4338)$ and $P^{\Lambda}_{\psi s}(4255)$ poles, as summarized in Table I; J^P is consistent with the LHCb's result for $P^{\Lambda}_{\psi s}(4338)$. In the table, we also list the Riemann sheets of the poles by $(s_{\Lambda_c\bar{D}_s}s_{\Xi_c^0\bar{D}^0}s_{\Xi_c^+D^-})$ where $s_\alpha=p$ or u depending on whether the pole is located on the physical (p) or unphysical (u) sheet of a channel α.[3] The pole locations relative to the relevant thresholds are illustrated in Fig. 4. The $P^{\Lambda}_{\psi s}(4338)$ pole is mainly generated by $v_{\Xi_c\bar{D},\Xi_c\bar{D}}$. In fact, if $v_{\Xi_c\bar{D},\Lambda_c\bar{D}_s}$ is turned off, we find a $\Xi_c\bar{D}$ bound pole at 4334.9 MeV. On the other hand, $v_{\Lambda_c\bar{D}_s,\Lambda_c\bar{D}_s}$ alone is not strong enough to create a $\Lambda_c\bar{D}_s$ bound state but a virtual pole at 4251.8 MeV.

A light vector-meson exchange would (not) cause a strong attraction in $v_{\Xi_c\bar{D},\Xi_c\bar{D}}$ ($v_{\Lambda_c\bar{D}_s,\Lambda_c\bar{D}_s}$) [21]. A possible mechanism to cause the relatively strong $v_{\Lambda_c\bar{D}_s,\Lambda_c\bar{D}_s}$ is a two-pion-exchange (TPE). TPE mechanisms could be important to understand possible bound states of a bottomonia-pair [49] and a J/ψ-J/ψ pair [50]. Also, a lattice QCD [51] found that a TPE is the dominant long-range part of the ϕ-nucleon interaction, causing a large attraction. In addition, a K^*-exchange $\Lambda_c\bar{D}_s\to\Xi_c\bar{D}$ provides an attraction to $v_{\Xi_c\bar{D},\Lambda_c\bar{D}_s}$.

[3]Section 50 in Ref. [44] defines (un)physical sheet.

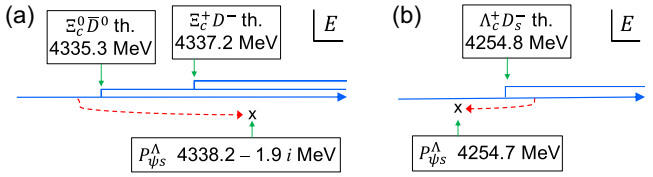

FIG. 4. Pole locations of (a) $P^{\Lambda}_{\psi s}(4338)$ and (b) $P^{\Lambda}_{\psi s}(4255)$ of the default model. The red dotted arrows indicate how to reach the poles from the closest physical energy regions. The double lines indicate the branch cuts.

As the LHCb analysis implies, the fluctuation at the $\Lambda_c\bar{D}_s$ threshold may be just statistical and $v_{\Lambda_c\bar{D}_s,\Lambda_c\bar{D}_s}$ might be weak. We thus consider an alternative model by removing $v_{\Lambda_c\bar{D}_s,\Lambda_c\bar{D}_s}$ from the default model, refit the data, and show its $M_{J/\psi\Lambda}$ distribution in Fig. 5 [blue]. The fit quality is $\chi^2/\mathrm{ndf}=(58+84+94+30)/(235-8)\simeq1.19$, similar to the default fit. An ordinary $\Lambda_c\bar{D}_s$ threshold cusp without a nearby pole is seen. The default and alternative models have $P^{\Lambda}_{\psi s}(4338)$ poles on different sheets; see Table I. This suggests that higher-statistics data should clarify whether a sharp peak exists at the $\Lambda_c\bar{D}_s$ threshold not only for probing $P^{\Lambda}_{\psi s}(4255)$ but also for constraining the $P^{\Lambda}_{\psi s}(4338)$ pole structure.

We also consider a case where the $\Xi_c\bar{D}$ interaction has an energy-dependence by replacing $h_{\Xi_c\bar{D},\Xi_c\bar{D}}$ in Eq. (3) with [52]

$$h_{\Xi_c\bar{D},\Xi_c\bar{D}}+h'_{\Xi_c\bar{D},\Xi_c\bar{D}}\frac{M^2_{J/\psi\Lambda}-(m_{\Xi_c}+m_{\bar{D}})^2}{2(m_{\Xi_c}+m_{\bar{D}})},\qquad(9)$$

and $h_{\Lambda_c\bar{D}_s,\Lambda_c\bar{D}_s}=0$. A comparable fit is obtained: $\chi^2/\mathrm{ndf}=(54+81+95+28)/(235-9)\simeq1.15$. This model generates three relevant $P^{\Lambda}_{\psi s}(4338)$ poles (Table I). A relatively

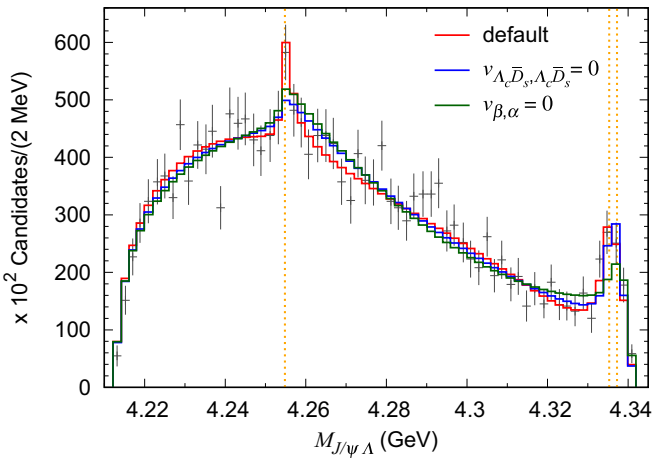

FIG. 5. Comparison of the default model with alternative ones where $v_{\Lambda_c\bar{D}_s,\Lambda_c\bar{D}_s}=0$ or $v_{\beta,\alpha}=0$ for all α, β in Eq. (3). Other features are the same as Fig. 3(a).

large width of the resonance (uuu) points to the importance of analyzing $\Xi_b^- \to J/\psi\Lambda K^-$ where the line shape would reflect the $P_{\psi s}^{\Lambda}(4338)$ pole positions more directly. In $B^- \to J/\psi\Lambda\bar{p}$, the line shape from $P_{\psi s}^{\Lambda}(4338)$ is distorted by the shrinking phase space. The different $P_{\psi s}^{\Lambda}(4338)$ poles would then be discriminated.

We finally examine if the $P_{\psi s}^{\Lambda}(4338)$ peak is caused merely by the $\Xi_c\bar{D}$ threshold cusp. A nonpole model, $h_{\beta,\alpha} = 0$ in Eq. (3), is fitted to the data and shown in Fig. 5 [green]. While the fit quality, $\chi^2/\mathrm{ndf} = (69 + 91 + 94 + 33)/(235 - 5) \simeq 1.25$, is not much worse than the above models overall, the fit in the $P_{\psi s}^{\Lambda}(4338)$ region is visibly worse. Thus, a nearby pole that enhances and sharpens the cusp is necessary to fit the data. We made a simple estimate of a statistical significance, and found that the existence of a nearby pole is favored by the LHCb data with 2.6σ significance; see the Supplemental Material [46] for details.

In Ref. [40], the authors proposed that the $P_{\psi s}^{\Lambda}(4338)$ peak might be caused by a mechanism involving a triangle singularity; no nearby pole exists. Within their model, however, the quality of fitting the $M_{J/\psi\Lambda}$ distribution data in the $P_{\psi s}^{\Lambda}(4338)$ peak region is similar to what our nonpole model does. Thus, the above conclusion should also apply to this triangle-singularity scenario. Yet, the nonpole cusp is sizable and, therefore, the pole should be located in a position where its impact on the line shape is considerably blocked by the $\Xi_c\bar{D}$ branch cut.

IV. SUMMARY

We analyzed the LHCb data on $B^- \to J/\psi\Lambda\bar{p}$ with diagrams in Fig. 1; weak B^- decays are followed by coupled-channel scatterings where $P_{\psi s}^{\Lambda}$ poles can be developed. Our default model simultaneously fits the $M_{J/\psi\Lambda}$, $M_{J/\psi\bar{p}}$, $M_{\Lambda\bar{p}}$, and $\cos\theta_{K^*}$ distributions; $\chi^2/\mathrm{ndf} \sim 1.21$. We found a $P_{\psi s}^{\Lambda}(4338)$ pole at $(4338.2 \pm 1.4) - (1.9 \pm 0.5)i$ MeV. This is the first-time pole determination of the first-discovered hidden-charm pentaquark with strangeness. While the pole determination is important in its own right, it also sets the primary basis for investigating the nature of $P_{\psi s}^{\Lambda}(4338)$. The data disfavors the $P_{\psi s}^{\Lambda}(4338)$ structure as just a kinematical effect. Our default model also fits the fluctuating data at the $\Lambda_c\bar{D}_s$ threshold, giving a virtual $P_{\psi s}^{\Lambda}(4255)$ pole at 4254.7 ± 0.4 MeV. We also considered alternative fits where $P_{\psi s}^{\Lambda}(4255)$ does not exist or the $\Xi_c\bar{D}$ interaction has an energy-dependence. We found $P_{\psi s}^{\Lambda}(4338)$ poles on different Riemann sheets (Table I). The future data should discriminate the different solutions.

ACKNOWLEDGMENTS

This work is in part supported by National Natural Science Foundation of China (NSFC) under Contracts No. U2032103 and No. 11625523 (S. X. N.) and under Grants No. 12175239 and No. 12221005 (J. J. W.), and also by National Key Research and Development Program of China under Contract No. 2020YFA0406400 (S. X. N., J. J. W.).

[1] H.-X. Chen, W. Chen, X. Liu, and S.-L. Zhu, The hidden-charm pentaquark and tetraquark states, Phys. Rep. **639**, 1 (2016).
[2] A. Hosaka, T. Iijima, K. Miyabayashi, Y. Sakai, and S. Yasui, Exotic hadrons with heavy flavors: X, Y, Z, and related states, Prog. Theor. Exp. Phys. **2016**, 062C01 (2016).
[3] R. F. Lebed, R. E. Mitchell, and E. S. Swanson, Heavy-quark QCD exotica, Prog. Part. Nucl. Phys. **93**, 143 (2017).
[4] A. Esposito, A. Pilloni, and A. D. Polosa, Multiquark resonances, Phys. Rept. **668**, 1 (2017).
[5] A. Ali, J. S. Lange, and S. Stone, Exotics: Heavy pentaquarks and tetraquarks, Prog. Part. Nucl. Phys. **97**, 123 (2017).
[6] F.-K. Guo, C. Hanhart, U.-G. Meißner, Q. Wang, Q. Zhao, and B.-S. Zou, Hadronic molecules, Rev. Mod. Phys. **90**, 015004 (2018).
[7] S. L. Olsen, T. Skwarnicki, and D. Zieminska, Nonstandard heavy mesons and baryons: Experimental evidence, Rev. Mod. Phys. **90**, 015003 (2018).
[8] N. Brambilla, S. Eidelman, C. Hanhart, A. Nefediev, C.-P. Shen, C. E. Thomas, A. Vairo, and C.-Z. Yuan, The XYZ states: Experimental and theoretical status and perspectives, Phys. Rep. **873**, 1 (2020).
[9] J.-J. Wu, R. Molina, E. Oset, and B.-S. Zou, Prediction of Narrow N^* and Λ^* Resonances with Hidden Charm above 4 GeV, Phys. Rev. Lett. **105**, 232001 (2010).
[10] J.-J. Wu, R. Molina, E. Oset, and B.-S. Zou, Dynamically generated N^* and Λ^* resonances in the hidden charm sector around 4.3 GeV, Phys. Rev. C **84**, 015202 (2011).
[11] S.-G. Yuan, K.-W. Wei, J. He, H.-S. Xu, and B.-S. Zou, Study of $qqqc\bar{c}$ five quark system with three kinds of quark-quark hyperfine interaction, Eur. Phys. J. A **48**, 61 (2012).
[12] R. Aaij *et al.* (LHCb Collaboration), Observation of $J/\psi p$ Resonances Consistent with Pentaquark States in $\Lambda_b^0 \to J/\psi K^-$ Decays, Phys. Rev. Lett. **115**, 072001 (2015).
[13] R. Aaij *et al.* (LHCb Collaboration), Observation of a Narrow Pentaquark State, $P_c(4312)^+$, and of Two-Peak Structure of the $P_c(4450)^+$, Phys. Rev. Lett. **122**, 222001 (2019).
[14] C.-W. Xiao, J. Nieves, and E. Oset, Prediction of hidden charm strange molecular baryon states with heavy quark spin symmetry, Phys. Lett. B **799**, 135051 (2019).

[15] H.-X. Chen, L.-S. Geng, W.-H. Liang, E. Oset, E. Wang, and J.-J. Xie, Looking for a hidden-charm pentaquark state with strangeness $S = -1$ from Ξ_b^- decay into $J/\psi K^-\Lambda$, Phys. Rev. C **93**, 065203 (2016).

[16] E. Santopinto and A. Giachino, Compact pentaquark structures, Phys. Rev. D **96**, 014014 (2017).

[17] C.-W. Shen, J.-J. Wu, and B.-S. Zou, Decay behaviors of possible $\Lambda_{c\bar{c}}$ states in hadronic molecule pictures, Phys. Rev. D **100**, 056006 (2019).

[18] R. Chen, J. He, and X. Liu, Possible strange hidden-charm pentaquarks from $\Sigma_c^{(*)}\bar{D}_s^*$ and $\Xi_c^{(\prime,*)}\bar{D}^*$ interactions, Chin. Phys. C **41**, 103105 (2017).

[19] B. Wang, L. Meng, and S.-L. Zhu, Spectrum of the strange hidden charm molecular pentaquarks in chiral effective field theory, Phys. Rev. D **101**, 034018 (2020).

[20] R. Aaij *et al.* (LHCb Collaboration), Evidence of a $J/\psi\Lambda$ structure and observation of excited Ξ^- states in the $\Xi_b^- \to J/\psi\Lambda K^-$ decay, Sci. Bull. **66**, 1278 (2021).

[21] C.-W. Xiao, J.-J. Wu, and B.-S. Zou, Molecular nature of $P_{cs}(4459)$ and its heavy quark spin partners, Phys. Rev. D **103**, 054016 (2021).

[22] F.-Z. Peng, M.-J. Yan, M. Sánchez Sánchez, and M. P. Valderrama, The $P_{cs}(4459)$ pentaquark from a combined effective field theory and phenomenological perspective, Eur. Phys. J. C **81**, 666 (2021).

[23] S. Clymton, H.-J. Kim, and H.-C. Kim, Production of hidden-charm strange pentaquarks P_{cs} from the $K^- p \to J/\psi\Lambda$ reaction, Phys. Rev. D **104**, 014023 (2021).

[24] Z.-G. Wang and Q. Xin, Analysis of hidden-charm pentaquark molecular states with and without strangeness via the QCD sum rules, Chin. Phys. C **45**, 123105 (2021).

[25] J.-X. Lu, M.-Z. Liu, R.-X. Shi, and L.-S. Geng, Understanding $P_{cs}(4459)$ as a hadronic molecule in the $\Xi_b^- \to J/\psi\Lambda K^-$ decay, Phys. Rev. D **104**, 034022 (2021).

[26] M.-W. Li, Z.-W. Liu, Z.-F. Sun, and R. Chen, Magnetic moments and transition magnetic moments of P_c and P_{cs} states, Phys. Rev. D **104**, 054016 (2021).

[27] X. Hu and J. Ping, Investigation of hidden-charm pentaquarks with strangeness $S = -1$, Eur. Phys. J. C **82**, 118 (2022).

[28] K. Chen, R. Chen, L. Meng, B. Wang, and S.-L. Zhu, Systematics of the heavy flavor hadronic molecules, Eur. Phys. J. C **82**, 581 (2022).

[29] C. Cheng, F. Yang, and Y. Huang, Searching for strange hidden-charm pentaquark state $P_{cs}(4459)$ in $\gamma p \to K^+ P_{cs}(4459)$ reaction, Phys. Rev. D **104**, 116007 (2021).

[30] H.-X. Chen, W. Chen, X. Liu, and X.-H. Liu, Establishing the first hidden-charm pentaquark with strangeness, Eur. Phys. J. C **81**, 409 (2021).

[31] Z.-G. Wang, Analysis of the $P_{cs}(4459)$ as the hidden-charm pentaquark state with QCD sum rules, Int. J. Mod. Phys. A **36**, 2150071 (2021).

[32] K. Azizi, Y. Sarac, and H. Sundu, Investigation of $P_{cs}(4459)^0$ pentaquark via its strong decay to $\Lambda J/\Psi$, Phys. Rev. D **103**, 094033 (2021).

[33] R. Chen, Can the newly $P_{cs}(4459)$ be a strange hidden-charm $\Xi_c\bar{D}^*$ molecular pentaquarks?, Phys. Rev. D **103**, 054007 (2021).

[34] M.-Z. Liu, Y.-W. Pan, and L.-S. Geng, Can discovery of hidden charm strange pentaquark states help determine the spins of $P_c(4440)$ and $P_c(4457)$?, Phys. Rev. D **103**, 034003 (2021).

[35] W.-Y. Liu, W. Hao, G.-Y. Wang, Y.-Y. Wang, E. Wang, and D.-M. Li, The resonances $X(4140)$, $X(4160)$, and $P_{cs}(4459)$ in the decay of $\Lambda_b \to J/\psi\Lambda\phi$, Phys. Rev. D **103**, 034019 (2021).

[36] LHCb Collaboration, Observation of a $J/\psi\Lambda$ resonance consistent with a strange pentaquark candidate in $B^- \to J/\psi\Lambda\bar{p}$ decays, arXiv:2210.10346.

[37] M. Karliner and J. R. Rosner, New strange pentaquarks, Phys. Rev. D **106**, 036024 (2022).

[38] F.-L. Wang and X. Liu, Emergence of molecular-type characteristic spectrum of hidden-charm pentaquark with strangeness embodied in the $P^{\Lambda}_{\psi s}(4338)$ and $P_{cs}(4459)$, Phys. Lett. B **835**, 137583 (2022).

[39] M.-J. Yan, F.-Z. Peng, M. S. Sánchez, and M. P. Valderrama, $P^{\Lambda}_{\psi s}(4338)$ pentaquark and its partners in the molecular picture, Phys. Rev. D **107**, 074025 (2023).

[40] T. J. Burns and E. S. Swanson, The LHCb state $P^{\Lambda}_{\psi s}(4338)$ as a triangle singularity, Phys. Lett. B **838**, 137715 (2023).

[41] F.-K. Guo, X.-H. Liu, and S. Sakai, Threshold cusps and triangle singularities in hadronic reactions, Prog. Part. Nucl. Phys. **112**, 103757 (2020).

[42] L. Meng, B. Wang, and S.-L. Zhu, The double thresholds distort the lineshapes of the $P^{\Lambda}_{\psi s}(4338)^0$ resonance, Phys. Rev. D **107**, 1 (2023).

[43] X.-K. Dong, F.-K. Guo, and B.-S. Zou, Explaining the Many Threshold Structures in the Heavy-Quark Hadron Spectrum, Phys. Rev. Lett. **126**, 152001 (2021).

[44] P. A. Zyla *et al.* (Particle Data Group), The review of particle physics, Prog. Theor. Exp. Phys. **2020**, 083C01 (2020).

[45] H. Kamano, S. X. Nakamura, T.-S. H. Lee, and T. Sato, Unitary coupled-channels model for three-mesons decays of heavy mesons, Phys. Rev. D **84**, 114019 (2011).

[46] See Supplemental Material at http://link.aps.org/supplemental/10.1103/PhysRevD.108.L011501 for parameter values, statistical significance of the $P^{\Lambda}_{\psi s}(4338)$ pole, which includes Ref. [47].

[47] O. Behnke, K. Kröninger, G. Schott, and T. Schörner-Sadenius, *Data Analysis in High Energy Physics—A Practical Guide to Statistical Methods* (Wiley-VCH Verlag GmbH & Co. KGaA, Germany, 2013).

[48] S. X. Nakamura, A. Hosaka, and Y. Yamaguchi, $P_c(4312)^+$ and $P_c(4337)^+$ as interfering $\Sigma_c\bar{D}$ and $\Lambda_c\bar{D}^*$ threshold cusps, Phys. Rev. D **104**, L091503 (2021).

[49] N. Brambilla, G. Krein, J. T. Castellà, and A. Vairo, Long-range properties of $1S$ bottomonium states, Phys. Rev. D **93**, 054002 (2016).

[50] X.-K. Dong, V. Baru, F.-K. Guo, C. Hanhart, A. Nefediev, and B.-S. Zou, Is the existence of a $J/\psi J/\psi$ bound state plausible? Sci. Bull. **66**, 2462 (2021).

[51] Y. Lyu, T. Doi, T. Hatsuda, Y. Ikeda, J. Meng, K. Sasaki, and T. Sugiura, Attractive N-ϕ interaction and two-pion tail from lattice QCD near physical point, Phys. Rev. D **106**, 074507 (2022).

[52] M.-L. Du, M. Albaladejo, F.-K. Guo, and J. Nieves, Combined analysis of the $Z_c(3900)$ and the $Z_{cs}(3985)$ exotic states, Phys. Rev. D **105**, 074018 (2022).